STRUCTURAL BIOLOGY COMMUNICATIONS

ISSN 2053-230X

Received 13 June 2019
Accepted 15 July 2019

Edited by K. K. Kim, Sungkyunkwan University School of Medicine, Republic of Korea

Keywords: RNA structure; fluorescence turn-on aptamers; X-ray free-electron lasers; *i*Mango-III; fluorescence; XFELS; room temperature.

PDB reference: *i*Mango-III, 6pq7

Supporting information: this article has supporting information at journals.iucr.org/f

Co-crystal structure of the *i*Mango-III fluorescent RNA aptamer using an X-ray free-electron laser

Robert J. Trachman III,[a] Jason R. Stagno,[b] Chelsie Conrad,[b] Christopher P. Jones,[a] Pontus Fischer,[c,d] Alke Meents,[c,d] Yun-Xing Wang[b] and Adrian R. Ferré-D'Amaré[a]*

[a]Biochemistry and Biophysics Center, National Heart, Lung and Blood Institute, Bethesda, Maryland, USA, [b]Structural Biophysics Laboratory, Center for Cancer Research, National Cancer Institute, Frederick, Maryland, USA, [c]Center for Free Electron Laser Science, DESY, Notkestrasse 85, 22607 Hamburg, Germany, and [d]DESY Photon Science, Notkestrasse 85, 22607 Hamburg, Germany. *Correspondence e-mail: adrian.ferre@nih.gov

Turn-on aptamers are *in vitro*-selected RNAs that bind to conditionally fluorescent small molecules and enhance their fluorescence. Upon binding TO1-biotin, the *i*Mango-III aptamer achieves the largest fluorescence enhancement reported for turn-on aptamers (over 5000-fold). This aptamer was generated by structure-guided engineering and functional reselection of the parental aptamer Mango-III. Structures of both Mango-III and *i*Mango-III have previously been determined by conventional cryocrystallography using synchrotron X-radiation. Using an X-ray free-electron laser (XFEL), the room-temperature *i*Mango-III–TO1-biotin co-crystal structure has now been determined at 3.0 Å resolution. This structural model, which was refined against a data set of ∼1300 diffraction images (each from a single crystal), is largely consistent with the structures determined from single-crystal data sets collected at 100 K. This constitutes a technical benchmark on the way to XFEL pump–probe experiments on fluorescent RNA–small molecule complexes.

1. Introduction

X-ray free-electron lasers (XFELs) are a source of both brilliant and coherent photons that are suitable for investigating the structures of macromolecules (Chapman, 2019). XFELs enable small and radiation-damage-prone crystals to be utilized in diffraction experiments to determine macromolecular structure. Moreover, small crystals are ideal for pump–probe or mix-and-inject serial femtosecond crystallography experiments to study structural kinetics (Stagno, Bhandari *et al.*, 2017; Stagno, Liu *et al.*, 2017; Schmidt, 2019).

X-ray free-electron laser scattering (XFELS) is ideally suited to study photoinduced changes in macromolecules (Schmidt, 2017). Fluorescence turn-on aptamers would benefit from study by XFELS. Co-crystal structures of several fluorescent aptamers have been determined in their fluorophore-bound states. These structures were determined using diffraction data from cryopreserved crystals obtained by conventional rotation photography with monochromatic synchrotron X-radiation, with ambient light present during sample manipulation and data collection (Trachman *et al.*, 2017, 2018, 2019; Warner *et al.*, 2014, 2017). Therefore, it is not clear what state, or mixture of states, is described by these X-ray crystallographic structures of fluorescent aptamers. Photoactive yellow protein undergoes conformational changes on the femtosecond timescale to promote an excited state and undergo radiative decay (Tenboer *et al.*, 2014; Pande *et al.*, 2016). Fluorescent aptamers may undergo similar structural

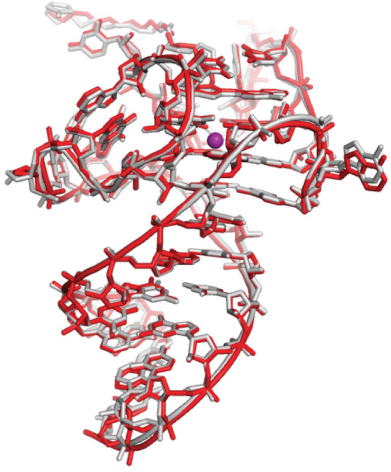

changes upon photoexcitation. In order to establish the technical feasibility of such experiments, we have determined the room-temperature co-crystal structure of the *i*Mango-III fluorescence turn-on aptamer at 3.0 Å resolution. The data set used to refine the structure resulted from merging ∼1300 diffraction images of microcrystals. The refined model superimposes closely with the 1.55 Å resolution crystal structure determined using data collected at 100 K.

2. Materials and methods

2.1. RNA purification and crystallization

The 37-nucleotide *i*Mango-III aptamer was chemically synthesized (Dharmacon), purified by electrophoresis on a 15% (19:1) polyacrylamide, 8 *M* urea, 1× TBE gel and electro-eluted. The RNA was exchanged into 20 m*M* MOPS–KOH pH 7.0, 150 m*M* KCl, 10 µ*M* EDTA using a Millipore concentrator with a 3 kDa cutoff followed by filtering through a 0.1 µm spin filter. The RNA was refolded by heating to 95°C for 3 min and allowing to cool on the bench. TO1-biotin was added to the *i*Mango-III solution in a 1:1 molar ratio of RNA to fluorophore. Crystals were grown by vapor diffusion. Sitting drops generated by mixing 0.2 µl of 200 µ*M* *i*Mango-III–TO1-biotin and 0.2 µl of a reservoir solution consisting of 0.1 *M* sodium cacodylate pH 7.1, 17.5%(*w*/*v*) polyethylene glycol (PEG) 3350, 0.25 *M* magnesium acetate were equilibrated against 60 µl reservoir solution at 21°C. Microcrystals of maximum dimensions ∼5–15 µm generally appeared within two days.

2.2. Sample preparation and data collection

Before transferring the microcrystals by pipetting, an equal volume of stabilizing solution consisting of the RNA folding buffer and reservoir solution supplemented with 15%(*v*/*v*) PEG 400 was added to each drop. The drops were combined and stored in a polypropylene microcentrifuge tube sandwiched between room-temperature cold packs en route to the beamline, where they were stored in a 21°C incubator until use. Upon arrival at the XFEL facility, visual inspection of the sample suggested that the crystals were intact.

The sample was prepared for data collection on a fixed-target Roadrunner goniometer as described previously (Roedig *et al.*, 2017). The Roadrunner chips were prepared from silicon wafers as described previously (Roedig *et al.*, 2017) and were washed with tetramethylammonium hydroxide and NH_4F/HF before use. 500 µl of crystal solution at a concentration of ∼100 microcrystals per microlitre was pipetted directly onto the center of a 31 000-pore silicon chip in a humidified chamber at room temperature. During sample application, the chip was wicked from the bottom with filter paper to draw crystals down into the pores, resulting in the sample covering the entire surface of the chip. After ∼5 min, the chip was stationed in the Roadrunner goniometer under a constant 92% humidity and scanned at a rate of ∼120 images per second. Samples were illuminated with a 527 nm laser pulse at a power of 5 mJ mm^{-2} for 100 ns immediately prior to X-ray photon scattering (τ = 0). Data were collected at 9516 eV with a 44 fs pulse duration on a Cornell–SLAC hybrid pixel-array detector operating at 120 Hz.

2.3. Data reduction and structure refinement

Images containing diffraction patterns were identified using *Cheetah* (Barty *et al.*, 2014), yielding 1328 images with potential Bragg reflections. The data were indexed using *CrystFEL* (White *et al.*, 2013). Initial indexing without supplying unit-cell parameters resulted in ∼1165 indexable images with a resolution range of 52.04–2.04 Å. Many of the indexed unit-cell parameters resembled the previously determined unit-cell parameters for this crystal form at 100 K (Trachman *et al.*, 2017). The resolution cutoff criterion was to include data from resolution shells with a CC* above 0.7 (*i.e.* $CC_{1/2}$ > ∼0.2; Karplus & Diederichs, 2015). The last shell to satisfy this criterion had a high-resolution limit of 2.8 Å.

Molecular replacement was performed with *Phaser* (McCoy *et al.*, 2007) using the previously determined *i*Mango-III structure with all ions and TO1-biotin removed as the search model (PDB entry 6e8u; Trachman *et al.*, 2019). Simulated-annealing, energy and individual *B*-factor refinement was performed in *PHENIX* (Adams *et al.*, 2010) using a 3.0 Å resolution cutoff. Refinement at lower resolution cutoffs (*e.g.* 3.0–4.0 Å) resulted in poorer free *R* factors. Additional rounds of refinement were interspersed with manual building in *Coot*. Figures were prepared using *PyMOL* (Schrödinger). Coordinates and structure factors have been deposited in the Protein Data Bank as PDB entry 6pq7.

3. Results and discussion

In the course of optimizing growth conditions for preparing large single crystals, microcrystals of the *i*Mango-III fluorescent aptamer with maximum dimensions of ∼5–15 µm were grown and pooled for XFELS experiments [Fig. 1(*a*)]. In addition to diffraction data collection using XFELS on microcrystals, the primary experimental difference between these and previous experiments are temperature (*i.e.* 293 and 100 K, respectively) and the potential hydration or dehydration that might occur during microcrystal sample application in the Roadrunner goniometer (Roedig *et al.*, 2017).

Although diffraction to ∼2.0 Å resolution was observed, the nominal resolution of the data set is ∼2.8 Å (Table 1), raising the possibility of obtaining a higher resolution in the future with a greater number of crystals. Indeed, data collection at cryo-temperatures resulted in diffraction to resolutions of higher than 1.5 Å. During data collection it was observed that the chip was not fully wicked, resulting in crystals dislodging from the wells, reducing the hit rate. Therefore, improvement of sample preparation and the hit rate could result in higher resolution data sets.

The structural model from the room-temperature XFELS experiment is consistent with the previously determined cryocrystallographic structure. Least-squares structural superposition of the refined models (all non-H atoms) confirmed a highly similar structure, with an r.m.s.d. of 0.28 Å

[Fig. 1(*a*)]. The crystal packing and unit-cell parameters are largely unperturbed by the increased temperature or laser excitation. Consistent with this, the *B* factors are highly similar throughout the structures (correlation coefficient of 0.70) [Fig. 1(*b*)]. To determine whether substantial structural changes occur in the TO1-biotin binding pocket, least-squares structural superposition of all non-H atoms of the ligand and locally adjoining residues (9, 10, 13, 14, 15, 18, 19, 21 and 22) was performed. The r.m.s.d. for this binding-pocket atom selection was 0.27, which is consistent with the overall superposition. Thus, given the coordinate precision of the structures from the maximum-likelihood estimation (0.16 and 0.40 Å for the cryocrystallographic and XFEL structures, respectively), the changes in experimental conditions did not significantly alter the *i*Mango-III RNA structure or its mode of fluorophore binding.

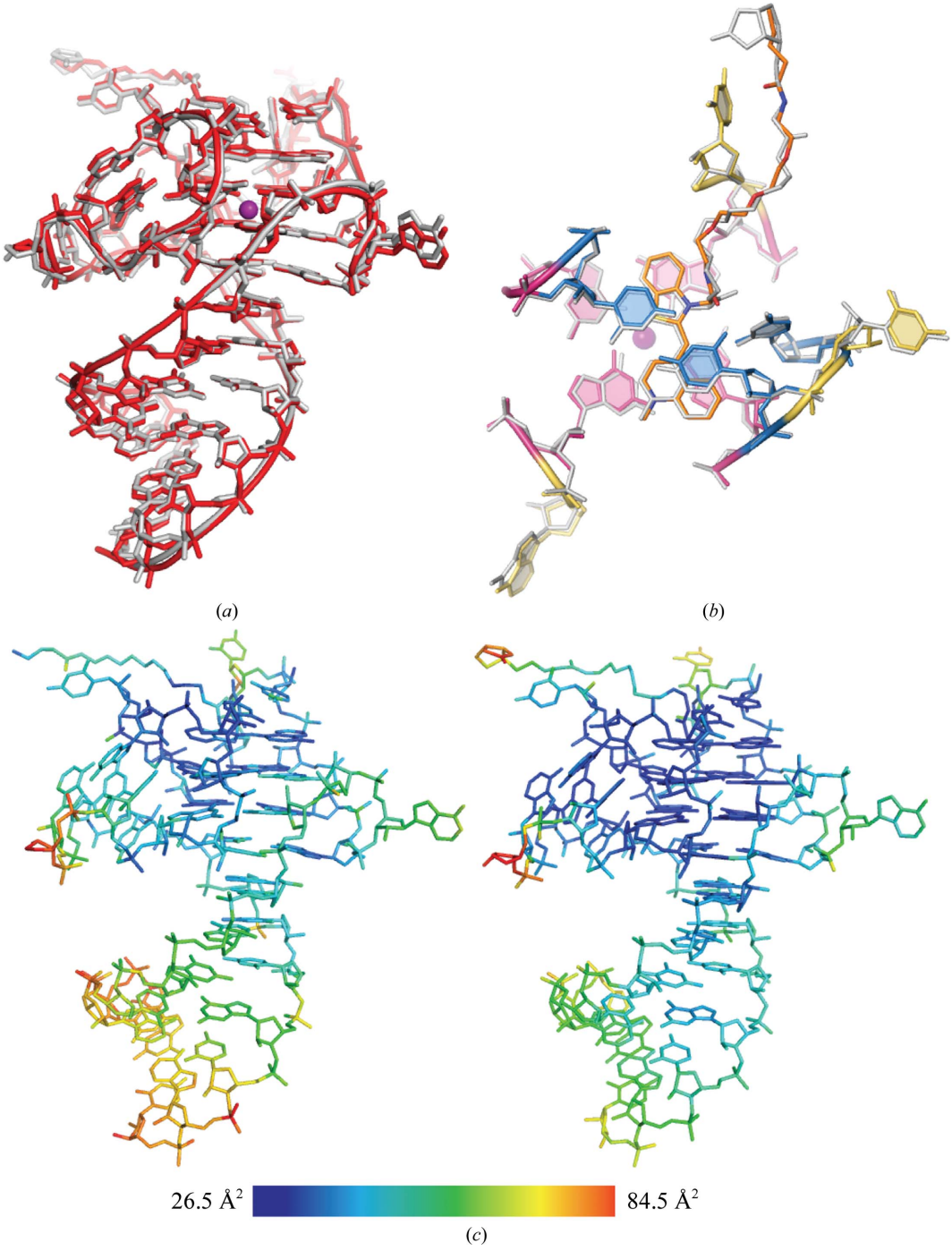

Figure 1
(*a*) Alignment of the *i*Mango-III aptamer structure determined by conventional X-ray crystallography at 100 K (gray) with the *i*Mango-III structure determined by XFELS at room temperature (red). The r.m.s.d. for all non-H atoms is 0.28 Å. (*b*) Structural alignment of the ligand-binding pocket residues. The r.m.s.d. for all non-H atoms is 0.27 Å. (*c*) *i*Mango-III XFELS (left) and *i*Mango-III cryo (right) structures colored by *B* factor. The color scale is shown at the bottom of the panel.

Table 1
Data-collection and refinement statistics.

Values in parentheses are for the highest resolution shell.

Data collection	
Wavelength (Å)	1.303
Collected frames	31000
Diffraction hits	1346
Indexed frames	1165
Resolution range (Å)	52.5–2.8
Space group	$I4_122$
Unit-cell parameters (Å, °)	$a = b = 53.6$, $c = 194.8$, $\alpha = \beta = \gamma = 90$
Total No. of reflections	164324 (2568)
No. of unique reflections	3816 (368)
$CC_{1/2}$	0.70 (0.245)
R_{split}† (%)	53.0 (142.1)
Completeness (%)	99.9 (100.0)
Multiplicity	3.0 (3.0)
Refinement	
Resolution range (Å)	52.5–3.0 (3.30–3.00)
R_{work}/R_{free} (%)	0.269 (0.2614)/0.304 (0.319)
No. of atoms	
RNA	796
Ligand	43
Ions/water	2
B factors (Å^2)	
RNA	45.7
Ligand	36.8
Ions/water	57.4
R.m.s. deviations	
Bond lengths (Å)	0.006
Bond angles (°)	1.141

† R_{split} is defined by *CrystFEL* (White *et al.*, 2013) to be a figure of merit between two halves of a data set corrected for the loss in multiplicity.

This work demonstrates the unperturbed structure of the *i*Mango-III–TO1-biotin complex upon laser illumination at room temperature. Owing to experimental limitations, the laser could only emit light at 527 nm. Although the excitation laser was not tuned to peak absorbance (506 nm), an excited state can result at the 527 nm wavelength. Although we could not resolve any differences in the structural changes upon excitation, photon scattering after a 100 ns pulse may result in uncoordinated structural changes in crystal lattice monomers, resulting in a structural ensemble that is nearly identical to the cryogenically determined structure. Therefore, this study cannot rule out that structural changes occur upon photoexcitation. However, in addition, this experiment was performed at room temperature with a pump laser delivering a heat load to the individual samples. The difference in temperature between the cryogenic and room-temperature structures is at least 193 K. Therefore, thermal energy alone does not result in a significant, observable, distortion of the crystal structure. Optimizing the delay in the pump–probe may reveal structural changes that are important for photoexcitation and radiative decay.

Acknowledgements

We thank the staff at the Linac Coherent Light Source for XFEL support. Author contributions are as follows. RJT prepared *i*Mango-III–TO1-biotin RNA and the crystals, RJT and CC prepared samples for data collection, PF and AM performed data collection, RJT and JRS processed the diffraction data, RJT refined the data, and RJT and ARF wrote the manuscript with input from all authors.

Funding information

This work was supported by the intramural programs of the National Cancer Institute and the National Heart, Lung and Blood Institute, NIH.

References

Adams, P. D., Afonine, P. V., Bunkóczi, G., Chen, V. B., Davis, I. W., Echols, N., Headd, J. J., Hung, L.-W., Kapral, G. J., Grosse-Kunstleve, R. W., McCoy, A. J., Moriarty, N. W., Oeffner, R., Read, R. J., Richardson, D. C., Richardson, J. S., Terwilliger, T. C. & Zwart, P. H. (2010). *Acta Cryst.* D**66**, 213–221.

Barty, A., Kirian, R. A., Maia, F. R. N. C., Hantke, M., Yoon, C. H., White, T. A. & Chapman, H. (2014). *J. Appl. Cryst.* **47**, 1118–1131.

Chapman, H. N. (2019). *Annu. Rev. Biochem.* **88**, 35–58.

Karplus, P. A. & Diederichs, K. (2015). *Curr. Opin. Struct. Biol.* **34**, 60–68.

McCoy, A. J., Grosse-Kunstleve, R. W., Adams, P. D., Winn, M. D., Storoni, L. C. & Read, R. J. (2007). *J. Appl. Cryst.* **40**, 658–674.

Pande, K., Hutchison, C. D. M., Groenhof, G., Aquila, A., Robinson, J. S., Tenboer, J., Basu, S., Boutet, S., DePonte, D. P., Liang, M., White, T. A., Zatsepin, N. A., Yefanov, O., Morozov, D., Oberthuer, D., Gati, C., Subramanian, G., James, D., Zhao, Y., Koralek, J., Brayshaw, J., Kupitz, C., Conrad, C., Roy-Chowdhury, S., Coe, J. D., Metz, M., Xavier, P. L., Grant, T. D., Koglin, J. E., Ketawala, G., Fromme, R., Šrajer, V., Henning, R., Spence, J. C. H., Ourmazd, A., Schwander, P., Weierstall, U., Frank, M., Fromme, P., Barty, A., Chapman, H. N., Moffat, K., van Thor, J. J. & Schmidt, M. (2016). *Science*, **352**, 725–729.

Roedig, P., Ginn, H. M., Pakendorf, T., Sutton, G., Harlos, K., Walter, T. S., Meyer, J., Fischer, P., Duman, R., Vartiainen, I., Reime, B., Warmer, M., Brewster, A. S., Young, I. D., Michels-Clark, T., Sauter, N. K., Kotecha, A., Kelly, J., Rowlands, D. J., Sikorsky, M., Nelson, S., Damiani, D. S., Alonso-Mori, R., Ren, J., Fry, E. E., David, C., Stuart, D. I., Wagner, A. & Meents, A. (2017). *Nature Methods*, **14**, 805–810.

Schmidt, M. (2017). *Struct. Dyn.* **4**, 032201.

Schmidt, M. (2019). *Int. J. Mol. Sci.* **20**, 1401.

Stagno, J. R., Bhandari, Y. R., Conrad, C. E., Liu, Y. & Wang, Y.-X. (2017). *FEBS J.* **284**, 3374–3380.

Stagno, J. R., Liu, Y., Bhandari, Y. R., Conrad, C. E., Panja, S., Swain, M., Fan, L., Nelson, G., Li, C., Wendel, D. R., White, T. A., Coe, J. D., Wiedorn, M. O., Knoska, J., Oberthuer, D., Tuckey, R. A., Yu, P., Dyba, M., Tarasov, S. G., Weierstall, U., Grant, T. D., Schwieters, C. D., Zhang, J., Ferré-D'Amaré, A. R., Fromme, P., Draper, D. E., Liang, M., Hunter, M. S., Boutet, S., Tan, K., Zuo, X., Ji, X., Barty, A., Zatsepin, N. A., Chapman, H. N., Spence, J. C. H., Woodson, S. A. & Wang, Y.-X. (2017). *Nature (London)*, **541**, 242–246.

Tenboer, J., Basu, S., Zatsepin, N., Pande, K., Milathianaki, D., Frank, M., Hunter, M., Boutet, S., Williams, G. J., Koglin, J. E., Oberthuer, D., Heymann, M., Kupitz, C., Conrad, C., Coe, J., Roy-Chowdhury, S., Weierstall, U., James, D., Wang, D., Grant, T., Barty, A., Yefanov, O., Scales, J., Gati, C., Seuring, C., Srajer, V., Henning, R., Schwander, P., Fromme, R., Ourmazd, A., Moffat, K., Van Thor, J. J., Spence, J. C. H., Fromme, P., Chapman, H. N. & Schmidt, M. (2014). *Science*, **346**, 1242–1246.

Trachman, R. J. III, Abdolahzadeh, A., Andreoni, A., Cojocaru, R., Knutson, J. R., Ryckelynck, M., Unrau, P. J. & Ferré-D'Amaré, A. R. (2018). *Biochemistry*, **57**, 3544–3548.

Trachman, R. J. III, Autour, A., Jeng, S. C. Y., Abdolahzadeh, A., Andreoni, A., Cojocaru, R., Garipov, R., Dolgosheina, E. V., Knutson, J. R., Ryckelynck, M., Unrau, P. J. & Ferré-D'Amaré, A. R. (2019). *Nature Chem. Biol.* **15**, 472–479.

Trachman, R. J. III, Demeshkina, N. A., Lau, M. W. L., Panchapakesan, S. S. S., Jeng, S. C. Y., Unrau, P. J. & Ferré-D'Amaré, A. R. (2017). *Nature Chem. Biol.* **13**, 807–813.
Warner, K. D., Chen, M. C., Song, W. J., Strack, R. L., Thorn, A., Jaffrey, S. R. & Ferré-D'Amaré, A. R. (2014). *Nature Struct. Mol. Biol.* **21**, 658–663.
Warner, K. D., Sjekloća, L., Song, W. J., Filonov, G. S., Jaffrey, S. R. & Ferré-D'Amaré, A. R. (2017). *Nature Chem. Biol.* **13**, 1195–1201.
White, T. A., Barty, A., Stellato, F., Holton, J. M., Kirian, R. A., Zatsepin, N. A. & Chapman, H. N. (2013). *Acta Cryst.* D**69**, 1231–1240.